



Fotouhi, S., Tabatabaeian, A., Lotfan, S., Farrokhhabadi, A. and Fotouhi, M. (2022) Investigating the Effect of Interface Angle and Ply Thickness on Mode II Delamination Behaviour of Carbon/Epoxy Laminated Composites. In: 20th European Conference on Composite Materials (ECCM20), Lausanne, Switzerland, 26-30 Jun 2022, (Accepted for Publication).

There may be differences between this version and the published version. You are advised to consult the publisher's version if you wish to cite from it.

<https://eprints.gla.ac.uk/269524/>

Deposited on: 22 April 2022

Enlighten – Research publications by members of the University of Glasgow
<https://eprints.gla.ac.uk>

INVESTIGATING THE EFFECT OF INTERFACE ANGLE AND PLY THICKNESS ON MODE II DELAMINATION BEHAVIOUR OF CARBON/EPOXY LAMINATED COMPOSITES

Sakineh. Fotouhi^a, Ali. Tabatabaeian^a, Saeid Lotfian^b, Amin. Farrokhbadi^c, Mohammad. Fotouhi^a

a: University of Glasgow, sakineh.fotouhi@glasgow.ac.uk

b: University of Strathclyde

c: Tarbiat Modares University

Abstract: *The effect of angle and thickness of plies are investigated on the fracture energy release rate (ERR) in mode II of carbon/epoxy prepreg laminated composites using finite element modelling. The ply's angle of = 0°, 22.5°, 30°, 45°, 60°, and 90° with 4 different thicknesses are investigated. The finite element modelling is done using the virtual crack closure technique (VCCT) to evaluate the asymmetric effect. The overall stiffness of the laminates is designed to have the least difference from the Mode II standard ASTM test. The results show that by increasing the thickness of the plies, the asymmetric effect and consequently the mode I/Mode II loading contribution is increased. The results show that ERR is decreased by increasing both angle and thickness of the plies. This understanding can help in designing composite materials with better delamination resistant properties under different loadings such as low-velocity impact.*

Keywords: Laminated composites; finite element modelling; ERR; Ply thickness effect; Ply angle effect

1. Introduction

Low-speed impact, manufacturing defects and other factors will cause interlaminar delamination that reduces the load-carrying capacity of laminated composites. Delamination is due to weakness in through-the-thickness direction of these laminates (1). Delamination resistance in terms of ERR or fracture toughness has been studied in different studies (2,3). Impact-induced delamination tends to be dominated by mode-II fracture (4). ASTM D7905 standard using end notch flexure (ENF) test is mostly used to calculate the mode II ERR (5). This standard is devoted to unidirectional laminated composites, being convenient with uniform crack growth and high contribution of mode II. Meanwhile, multidirectional laminates are mostly used in application and delamination occurs between plies of different angles (6). There are different studies on the mode II behaviour of multidirectional laminated composites. Chen et al. (7) investigated multidirectional carbon epoxy laminated composites with four kinds of ply angles (0°//−0°, 15°//−15°, 30°//−30°, and 45°//−45°) using the ENF test. They showed higher mode II ERR for variable angles of plies. Another ENF test on multidirectional carbon epoxy AS4/3501-6 laminated composites and 0// θ interfaces showed decreasing trend for energy release rate by increasing the off-axis angle (8). Marom et al. Showed a similar trend for mode II ERR for glass, carbon and kevlar laminated composites (9). Ozdil et al. (10) tested glass epoxy specimens with θ //− θ interfaces for delamination starter interfaces and showed three times ERR increasing for the angle variation from 0° to 45°. Pereira et al. (6) performed finite element and experimental analyses on glass epoxy ENF specimens with starter delamination on θ //− θ

and 0// θ interfaces. They reported increasing values for ERR mode II for both designed configurations by increasing θ .

Previous works show various issues and contradictory results for the mode II ERR of multidirectional laminated composites. Meanwhile, to the best knowledge of the authors, there is no comprehensive work on ply's angle and thickness effect on mode II ERR of laminated composites. In this study, the main objective is to study the angle and thickness effect simultaneously. Standard D7905/D7905M test is to calculate ERR mode II, G_{II} , using ENF test (11). According to this standard, unidirectional zero-degree plies of polymeric composites should be used for manufacturing the specimens to study a pure mode II behavior. When the delamination starter interface consists of different plies' angles, ERR is affected by bending-twisting and membrane-bending couplings (3,6) which generates asymmetric behavior. By generating asymmetric behavior, mode I contributes to the total ERR increases. Hence, in this study, thicker specimens are chosen to reduce the asymmetry effect.

2. Finite Element Modelling

Standard D7905/D7905M test is to calculate ERR mode II, G_{II} , using end-notched flexure (ENF) test (11). According to this standard, unidirectional zero-degree plies of polymeric composites should be used for manufacturing the specimens to study a pure mode II behavior. When delamination starter interface consists of different plies' angle, ERR is affected by bending-twisting and membrane-bending couplings (3,6) which generates asymmetric behavior. By generating asymmetric behavior, mode I contribution to the total ERR increases. Hence, in this study thicker specimens are chosen to reduce asymmetry effect. The samples consist of 32 plies with an overall thickness of 4 mm. The stacking sequences of $[0_{16-n}/\theta_n//0_{16}]$ and ply's angle of $\theta = 0^\circ, 22.5^\circ, 30^\circ, 45^\circ, 60^\circ,$ and 90° are chosen (see Figure 1). Where n indicates the non-zero layer' number being 1 to 4 and // indicates the location of the inserted crack.



Figure 1. Schematic of the designed specimens

Modelling was constructed by Abaqus software 3D 8-node brick elements. As it is shown in Figure 2 schematically, ENF specimens have been modelled with the length and width of 125 and 25 mm respectively. 30 mm crack length is considered from the supporting roller to the end of the crack and the span between the supporting rollers is 100 mm. A displacement of 4 mm was applied on the specimen and a general static solver was employed. Material property was defined for IM7/8552 carbon/epoxy pre-pregs according to Table 1.

Table 1. Material properties of IM7/8552

| | |
|------------------------------------|------------------------------------|
| $E_{11} = 161\text{Gpa}$ | $E_{22} = E_{33} = 11.4\text{Gpa}$ |
| $\nu_{12} = 0.3$ | $\nu_{13} = 0.436$ |
| $G_{12} = G_{13} = 5.17\text{GPa}$ | $G_{23} = 3.98\text{GPa}$ |

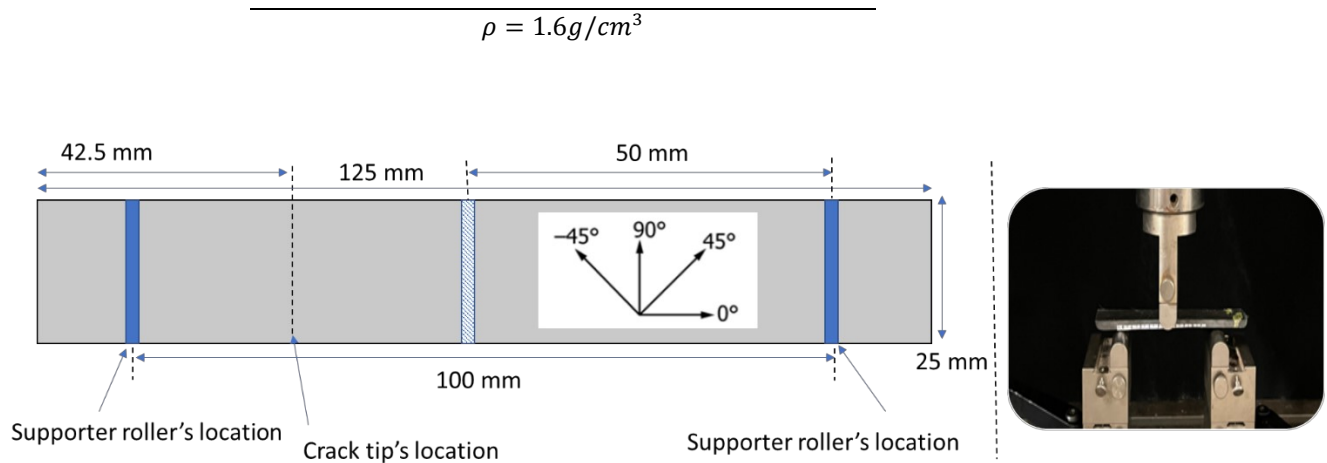


Figure 2. Schematic the ENF test and an experimental view of a ENF test.

Local basic single mesh was applied on the length of the specimens to reduce the element size around the crack tip to get accurate results (see Figure 3). Whole of the specimen was meshed with 8-node linear brick, reduced integration, and hourglass control (C3D8R).

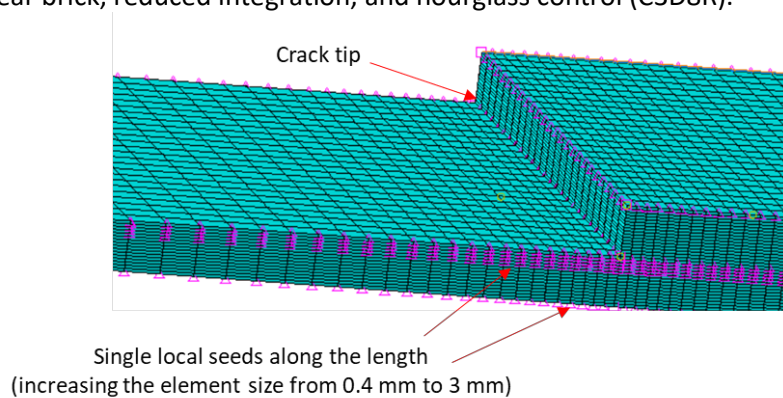


Figure 3. A zoomed area: smaller mesh sizes approaching the crack tip.

To calculate the ERR mode I, mode II, and mode III, i.e., G_I , G_{II} , and G_{III} , Virtual Crack Closure Technique (VCCT) was used. Normal behaviour with hard contact and tangential behaviour with a friction coefficient of 0.3 was defined for the interaction property between the rollers and the specimen. Small sliding and finite sliding were also employed for the cracked surfaces and the rest of the interactions respectively. The energy release rates are calculated using Eq. (1) to Eq. (3), the components of the equations are shown in Figure 4.

$$G_I = \frac{1}{2\Delta A} R_Y \Delta v \quad (1)$$

$$G_{II} = \frac{1}{2\Delta A} R_X \Delta u \quad (2)$$

$$G_{III} = \frac{1}{2\Delta A} R_Z \Delta w \quad (3)$$

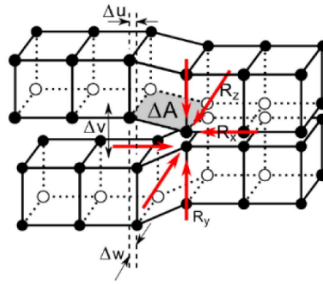


Figure 4. Crack geometry to calculate ERR using VCCT method (12).

3. Results and discussion

Load displacement graphs in Figure 5 show that changing angle and thickness of the plies affect the elastic response. By replacing the central plies' angle, elastic stiffness of the specimens is decreased, and this exceeds by increasing the plies' thickness as well. Table 2 show the maximum load achieved for each of the specimens and

Table 3 indicates how much the elastic response/maximum load varies by changing the angle and thickness of the plies. For the sample with lower angles i.e., 22.5° and 30°, this variation is up to 10% for all the thicknesses, while it is doubled for 90° specimens, reaching 16.20% for the specimen with four 90° plies.

Table 2. Maximum load of each of the specimens (extracted form Figure 5)

| $n \backslash \theta^\circ$ | 1 | 2 | 3 | 4 |
|-----------------------------|---------|---------|---------|---------|
| 22.5 | 22.8744 | 22.314 | 22.3444 | 21.4417 |
| 30 | 22.717 | 22.0542 | 21.4312 | 20.9232 |
| 45 | 22.485 | 21.6495 | 20.9185 | 20.3314 |
| 60 | 22.3444 | 21.4463 | 20.6502 | 20.0332 |
| 90 | 22.2383 | 21.2739 | 20.4143 | 19.5966 |

*Units are in N and maximum load for the standard (all zero) ENF test is 23.39 N.

Table 3. Stiffness/maximum load difference in % vs the standard (all zero) ENF test's configuration for each of the specimens.

| $n \backslash \theta^\circ$ | 1 | 2 | 3 | 4 |
|-----------------------------|------|------|-------|-------|
| 22.5 | 2.20 | 4.60 | 4.45 | 8.30 |
| 30 | 2.87 | 5.70 | 8.36 | 10.50 |
| 45 | 3.85 | 7.43 | 10.55 | 13.06 |
| 60 | 4.46 | 8.30 | 11.70 | 14.34 |
| 90 | 4.90 | 9.00 | 12.70 | 16.20 |

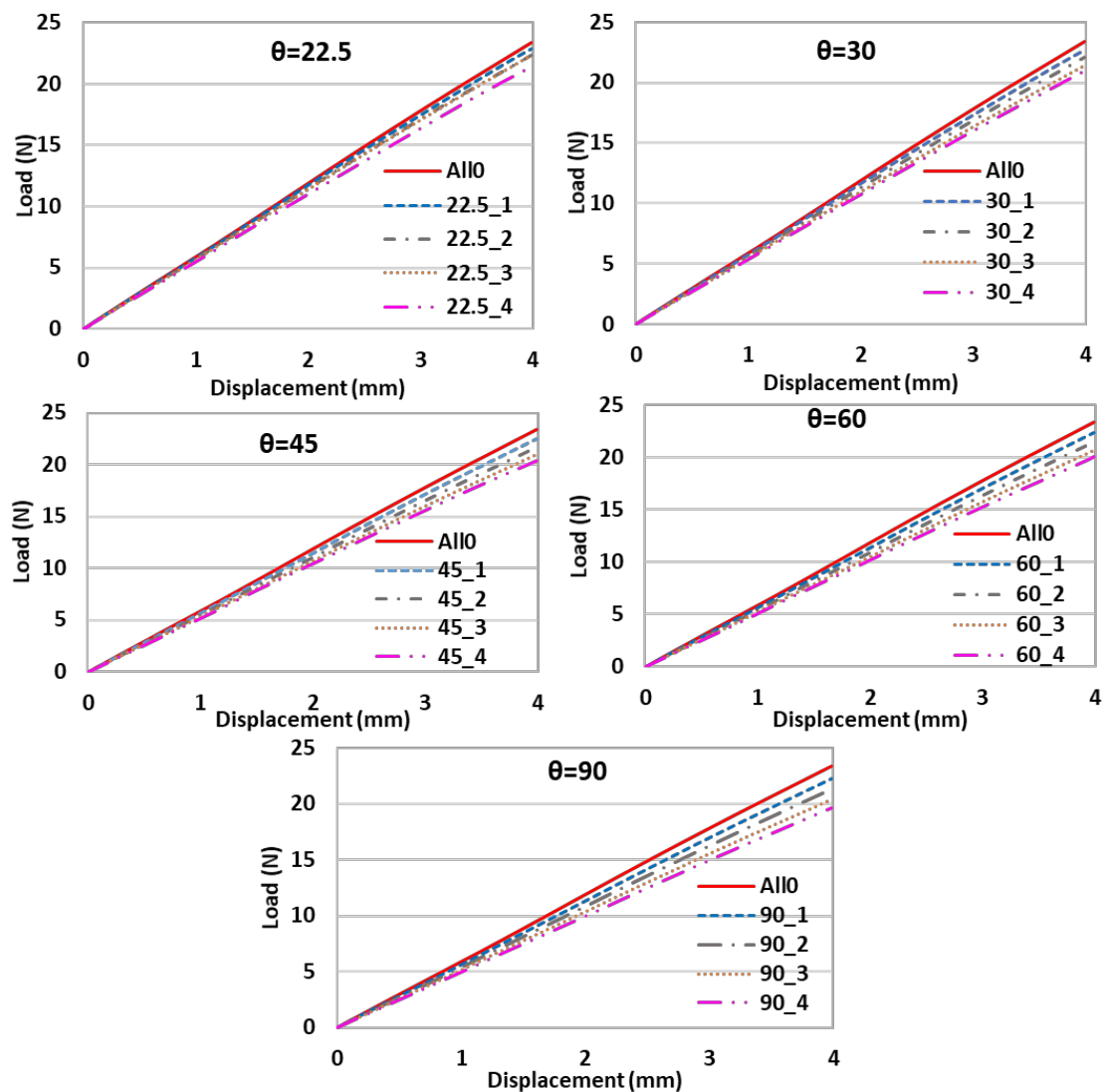


Figure 5. Load displacement graphs of the investigated specimens.

In addition to load and stiffness, energy release rate behavior is investigated. Mode III contribution is negligible for all the specimens. As an example, Figure 6 shows GIII distribution over total ERR (GIII+GII+GI) for the specimen with four 90° plies (90_4) as the extreme case in this study. GIII proportion is around 2.5 percent at the edges of the specimen which reaches rapidly to around zero at the central part of the crack tip. Distribution of GI/GII is shown in Figure 7. The figure shows GI proportion increases with increasing the ply angle and thickness for all the specimens. For the angles of 22.5° to 60°, except for the edges (due to edge effect), the average of this proportion is under 10% for all the ply's thicknesses, but for the 90_4 specimens, this proportion reaches to around 13%. These figures show the current study as a fair one to understand ply and thickness effect on GII behavior.

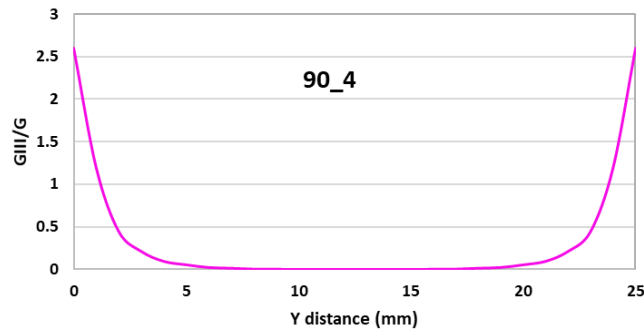


Figure 6. Mode III ratio ($G_{III}=G$) along the width of the specimen at the crack tip.

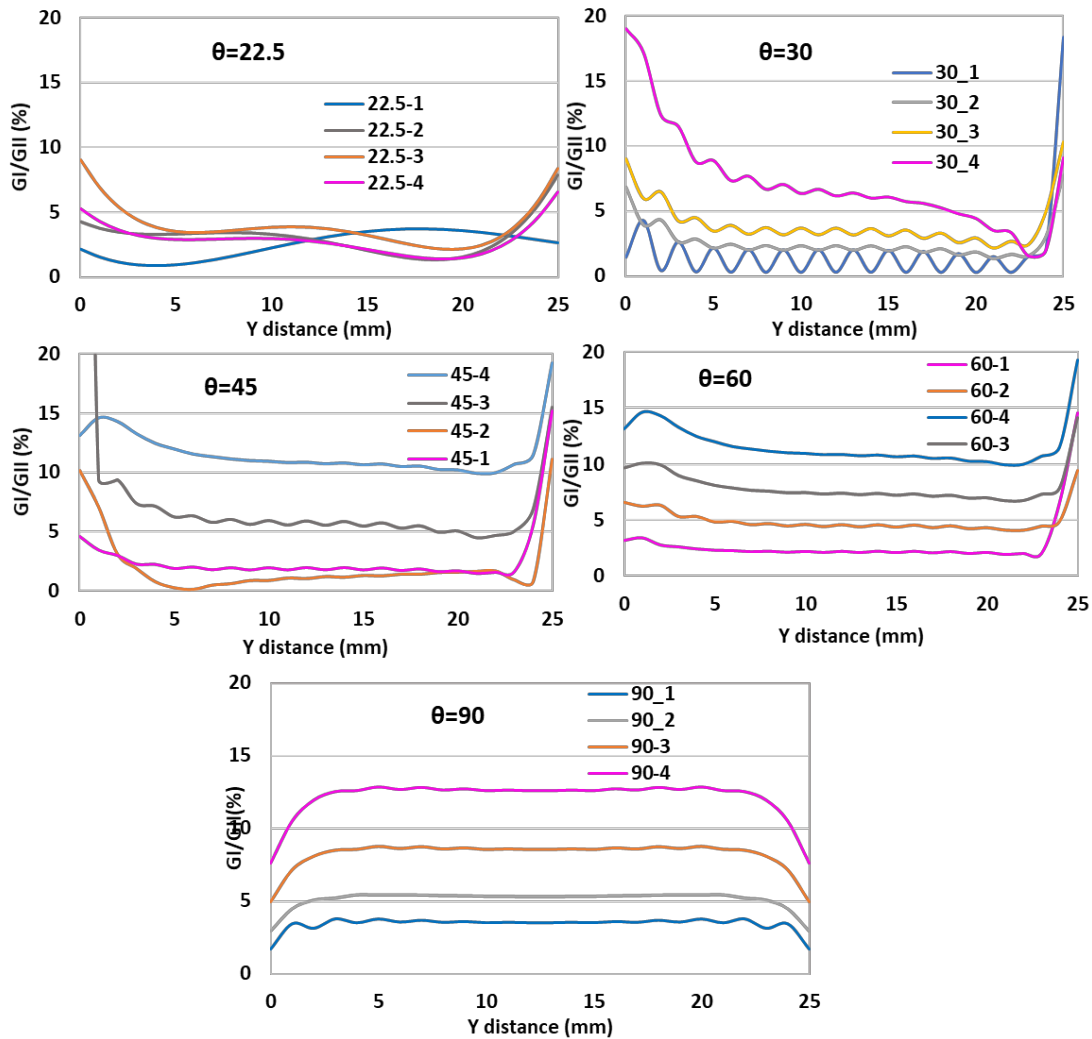


Figure 7. Mode I to mode II ratio ($G_I=G_{II}$) along the width of the specimens at the crack tip.

Distribution of G_{II}/G at the crack tip is presented in Figure 8. There is usually an oscillatory distribution for the stress component of delamination between plies of different angle. This mostly depends on the crack closure increment (6,13). The G_{II}/G graphs show that oscillatory behavior is more considerable for the lower angles i.e. 22.5° and 30° (see Figure 8). Hence, for the specimen with 22.5° plies, the graphs are smoothed for better demonstration. The average mode II proportion is above 90% of the total ERR except for specimen 90_4, showing a high

contribution of mode II. The higher the plies' degree, the smoother behavior is visible for the specimens.

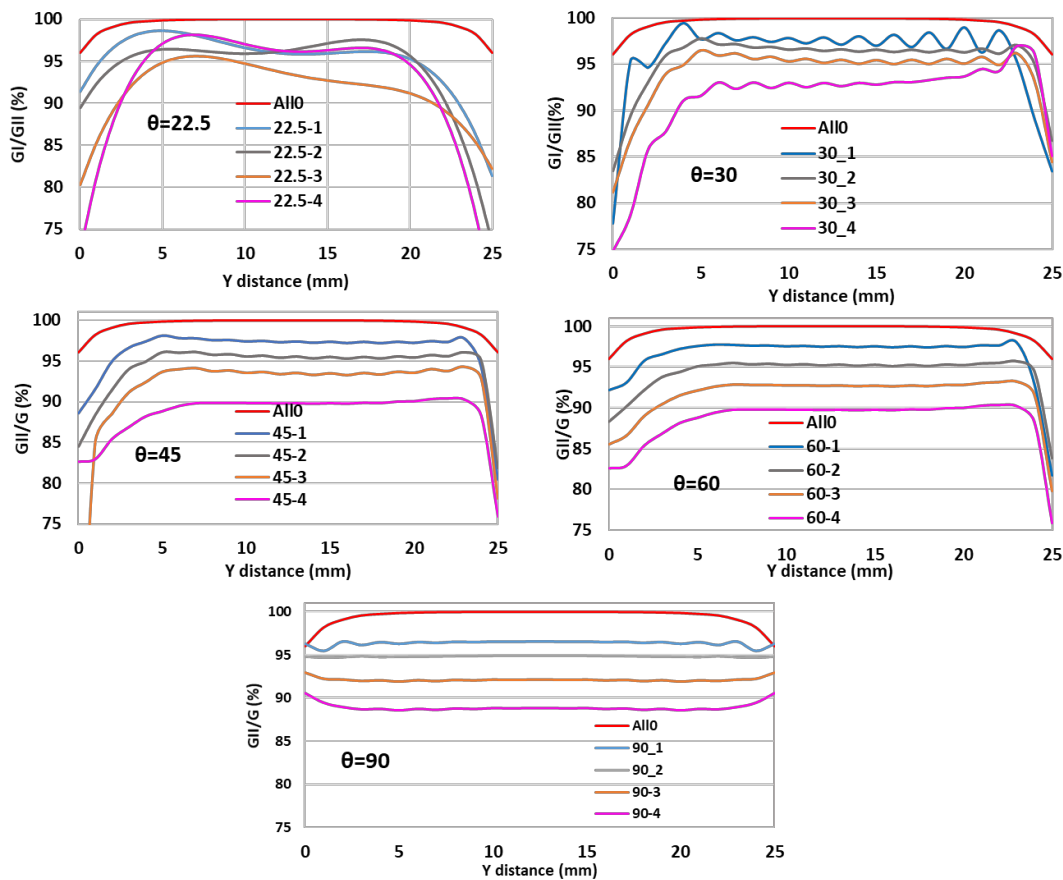


Figure 8. Mode II ratio ($G_{II}=G$) along the width of the specimens at the crack tip

It is noteworthy that, the specimens with 90-degree plies show different behavior for G_{II}/G distribution. For all the plies' angles, there is a high value at the edges of the crack, but the 90° specimen have a converse behavior. At the crack edges, contribution of mode II is higher than the central part of the crack tip.

4. Conclusions

This study aimed to investigate the effect of interface angle and thickness of the adjacent plies on the delamination behaviour of ENF specimens using finite element method. ENF specimens with configuration of $[0_{16-n}/\theta_n//0_{16}]$ where $\theta = 0^\circ, 22.5^\circ, 30^\circ, 45^\circ, 60^\circ, \text{ and } 90^\circ$, and $n=1, 2, 3, 4$ were modelled based on ASTM standard test. Afterwards, VCCT technique was used to calculate ERR for modes I, II, and III. Mode III proportion was negligible and mode I proportion was roughly under 10% for the specimens apart from the specimen with $n=4$ and $\theta=90^\circ$. It is concluded that the ERR value of $0//0$ interface were larger than those of the other interfaces. Furthermore, maximum load and stiffness of the specimens decreased by changing the plies' angle and increasing the thickness.

Acknowledgements

This work was funded under the UK Engineering and Physical Sciences Research Council (EPSRC) Grant EP/V009451/1 on Next generation of high-performance impact resistant composites with visibility of damage. The data necessary to support the conclusions are included in the paper.

5. References

1. Liu C, Gong Y, Gong Y, Li W, Liu Z, Hu N. Mode II fatigue delamination behaviour of composite multidirectional laminates and the stress ratio effect. *Eng Fract Mech.* 2022;264.
2. Chai H. Bond thickness effect in mixed-mode fracture and its significance to delamination resistance. *Int J Solids Struct.* 2021;219–220:63–80.
3. Davidson BD, Krüger R, König M. Effect of stacking sequence on energy release rate distributions in multidirectional DCB and ENF specimens. *Eng Fract Mech.* 1996;55(4):557–69.
4. Davies GAO, Zhang X. Impact damage prediction in carbon composite structures. *Int J Impact Eng.* 1995;16(1):149–70.
5. Li Z, Wang Z, Lu W, Zhou X, Suo T. Loading rate dependence of mode II fracture toughness in laminated composites reinforced by carbon nanotube films. *Compos Sci Technol.* 2021;215.
6. Pereira AB, De Morais AB. Mode II interlaminar fracture of glass/epoxy multidirectional laminates. *Compos Part A Appl Sci Manuf.* 2004;35(2):265–72.
7. Liu C, Bai R, Lei Z, Di J, Wu W, Zou J, et al. Mode II fracture toughness related to ply angle for composite delamination analysis. *Mech Adv Mater Struct.* 2021;28(23):2417–28.
8. Tao J, Sun CT. Influence of ply orientation on delamination in composite laminates. *J Compos Mater.* 1998;32(21):1933–47.
9. Marom G, Roman I, Harel H, Rosensft M, Kenig S, Moshonov A. The strain energy release rate of delamination in fabric-reinforced composites. *Int J Adhes Adhes.* 1988;8(2):73–4.
10. Ozdil F, Carlsson LA, Davies P. Beam analysis of angle-ply laminate end-notched flexure specimens. *Compos Sci Technol.* 1998;58(12):1929–38.
11. ASTM D7905. Standard test method for determination of the mode II interlaminar fracture toughness of unidirectional fiber-reinforced polymer matrix composites. *Astm.* 2014;1–18.
12. Gliszczynski A, Wiącek N. Experimental and numerical benchmark study of mode II interlaminar fracture toughness of unidirectional GFRP laminates under shear loading using the end-notched flexure (ENF) test. *Compos Struct.* 2021;258.
13. Chow WT, Atluri SN. Stress intensity factors as the fracture parameters for delamination crack growth in composite laminates. *Comput Mech.* 1998;21(1):1–10.